

<https://doi.org/10.1590/2318-0331.292420230113>

## Dam-break due to overtopping failure: experiments in homogeneous earthfill dams

### *Experimentos de ruptura de barragens de terra homogêneas por galgamento*

Bianca dos Santos Von Ahn<sup>1</sup>  & Rafael Manica<sup>1</sup> 

<sup>1</sup>Núcleo de Estudos em Correntes de Densidade, Instituto de Pesquisas Hidráulicas, Universidade Federal do Rio Grande do Sul, Porto Alegre, RS, Brasil

E-mails: b.vonahn@hotmail.com (BSVA), manica@iph.ufrgs.br (RM)

Received: November 04, 2023 - Revised: January 15, 2024 - Accepted: February 22, 2024

#### ABSTRACT

This work physically simulates the effect of low and high flow rates and filling times of reservoirs and rupture due to overtopping (caused by intense rains) of small homogeneous silty-sand earthfill dams. The experiments seek to verify how input variations impact the formation of the breach and the rupture wave. The results show that different filling times, soil moisture and composition, and degree of compaction affect landfill saturation, failure time, and breach formation. The result confirms that smaller breaches with a higher degree of compaction led to a lower peak rupture flow compared to dams with low degree of compaction. The rupture hydrograph presents a faster descent stage than an exponential hydrograph. Simulations and models based on this law may minimize the effect of the dam-break wave, also impacting water resource decision-making for damage reduction. The results were extrapolated to a real prototype, providing information and a database for the studies of overtopping dam-break waves.

**Keywords:** Small homogeneous earthfill dam; Overtopping dam failure; Dam breach; Physical modeling; Dynamic similarity.

#### RESUMO

Este trabalho simula fisicamente o efeito de baixas e altas vazões e tempos de enchimento de reservatórios e ruptura por galgamento (devido a chuvas intensas) de barragens homogêneas de aterro de areia siltica. Os experimentos buscam verificar como essas condições impactam na formação da ruptura e da onda de ruptura. Os resultados mostram que diferentes tempos de enchimento, umidade e composição do solo e grau de compactação afetam a saturação, o tempo de falha e a formação de brechas. O resultado confirma que brechas menores com maior grau de compactação levaram a um menor pico de vazão de ruptura. O hidrograma de ruptura apresenta uma etapa de descida mais rápida que um hidrograma exponencial. Simulações e modelos baseados nesta lei podem estar minimizando o efeito da onda de rompimento de barragens, impactando também a tomada de decisões sobre recursos hídricos. Os resultados foram extrapolados satisfatoriamente para um protótipo real, fornecendo um banco de dados para este tipo de estudo.

**Palavras-chave:** Pequenas barragens de terra homogêneas; Rompimento de barragem por galgamento; Brecha; Modelagem física; Semelhança dinâmica.

## INTRODUCTION

Dams are artificial obstacles built in watercourses with the purpose of retaining water, other liquids, tailings or debris. These are structures built by man since thousands of years ago allowing the development of essential activities in cities (Bassel, 1904; Kutzner, 1997). Dams present different types and sizes and they have different purposes, e.g. flood control, water retention for hydroelectric energy, human supply, industrial use and irrigation of agricultural lands (Gaioto, 2003). The most common type of dam found throughout the world is a homogeneous earthfill dam (Stephens, 2011; Alzamily & Abed, 2022), i.e. filled with only one type of borrow material (e.g. clay, silt and sand) without any complex prior processing (Kutzner, 1997). These structures are subject to failures, accidents (caused by partial or total collapse of the structure with uncontrollable release of the contents of a reservoir) and incidents (any occurrence that affects the behavior of the structure) that can lead to major disaster (Jansen, 1983; World Commission on Dams, 2000; Pereira, 2017).

Most of these failure events (accidents) occur due to overtopping flow caused by excess rain and insufficiency of spillway capacity, i.e. flow exceeding that established in the project (Collischonn & Tucci, 1997; Zhang et al., 2009; Pereira, 2017; Agência Nacional de Águas e Saneamento Básico, 2022). When a dam fails due to overtopping, millions of cubic meters of water overflow, flowing downstream at high velocity, and resulting in a dam-break wave (rupture hydrograph) with a high potential for destruction (Wylam, 2016). In fact, the overtopping flow causes a deep cut at the top of the crest and erosion on the downstream slope called breach (Galeano, 2016). Then, a dam-break wave produces a peak flow ( $Q_p$ ) characterized by the highest value obtained at a given instant ( $t_p$ ) (Faria et al., 2019; Campos, 2020).

In recent decades, major accidents and incidents involving dams. Zhang et al. (2009) analyzed more than 900 cases of occurrence of failures in dams located in several countries, where 66% occurred in earth dams. In Brazil, according to data from the National Water and Basic Sanitation Agency (ANA), there are 22,654 dams registered in the National Dam Safety Information System (SNISB). Between 2020 and 2021, 57 dam accidents were reported, and 22 occurred in earth dams due to overtopping (Agência Nacional de Águas e Saneamento Básico, 2021, 2022). Pereira (2017) demonstrated the necessity for studies and projects, as well as constant supervision, monitoring and maintenance of dam structures. However, the lack of technical information about the majority of these small dam failures (e.g. excess of precipitation and overtopped flow discharge, water depth on top of the dam, total time of dam failure, breach opening and time of emptying of the reservoir) causes difficulty in understanding thoroughly the phenomenon and is still an obstacle to understand and characterize these structures in intense rain events (Neiva Rodrigues et al., 2007; Guireli Netto et al., 2020; Fonseca, 2021). Understanding how these variations in precipitation (i.e. flow discharge), and consequently time of filling/emptying of the reservoir impacts the dam structure and operation is always necessary to enhance the knowledge of the present state of art, particularly related to small earth dams.

Pereira (2017) also stated that hydraulic dam projects must be supported by studies/tests in a physical model, to carry out

spillway capacity and flow energy dissipation tests (downstream erosive processes). In fact, physical models or reduced-scale models integrate the study of the flow with complex hydraulic structures (Motta, 1972; Marques & Unas, 2010; Aureli et al., 2021, 2023; Trautwein et al., 2022) mainly through cause-consequence scenarios of simulation. Several parameters are the main focus on the present state of art, including soil composition (Correia et al., 2018; Alzamily & Abed, 2022; Trautwein et al., 2022) and the understanding of the phenomenon of failure due to overtopping (inflow hydrograph), erosion (Saliba, 2009), deformation and seepage (Marques & Unas 2010; Jorge, 2013; Oliveira et al., 2018; Correia et al., 2018; Campos, 2020; Trautwein et al., 2022; Alzamily & Abed, 2022), breach formation and evolution (Pickert et al., 2011; Hanson et al., 2005; Luo et al., 2014; Campos, 2020). Franca (2002) highlighted that two phenomena require attention when choosing the scales in physical modelling: a) the inflow rate overtopping the dam and b) the percolation flow inside the body of the dam. Duarte et al. (2021) also stated that the knowledge of the maximum flows (inflow rate) in the river basins, related to a hydrological risk (return period), is an essential factor in the design of hydraulic structures, including earth dams. In fact, these parameters are important to adequately estimate a dam inflow and break wave (rupture) hydrograph (duration, shape, volume and peak flow) that is the closest to a real rupture (Campos, 2020).

Based on this experience, we directed this work to investigate two parameters described above and developed a methodology to replicate this phenomenon in the lab. Then, we analyze the effect of various inflow rates and reservoir filling times on overtopping flow failure in small homogeneous earthfill dams, using physical modeling experiments. A small-scale model of a hypothetical earth dam was built in which three- controlled physical simulations were carried out with low and high inflow rates in order to compare the cause-consequences scenarios in terms of hydraulics and their impacts on the dam structure. We also extrapolated the results obtained in the laboratory to a real hypothetical prototype. Finally, based on these controlled measured results and observations, we provide subsidies and a database about the potential impacts in case of a dam failure, enhancing understanding in the field of engineering.

## APPARATUS AND METHODS

### Apparatus

The homogeneous earthfill dam (Figure 1) without internal filter or upstream sealing was built inside a horizontal glass flume (Figure 1a) measuring 4.0 m long and 0.97 m wide. An acrylic box divided in two sections in the first 2 m, and 0.5 m in height delimited the fixed bed reservoir (Figure 1b). The total volume of the dam reservoir was 0.26 m<sup>3</sup>.

An auxiliary reservoir was responsible for the continuous supply of water through a water pipe to the system during the simulation. A Siemens® electromagnetic flow meter was installed on the inlet pipe to measure the injected discharge and volume into the reservoir, creating an inflow hydrograph (flow over time). Then, we were able to check the inflow rate and characterize the reservoir filling time. Two iPad cameras were positioned at the

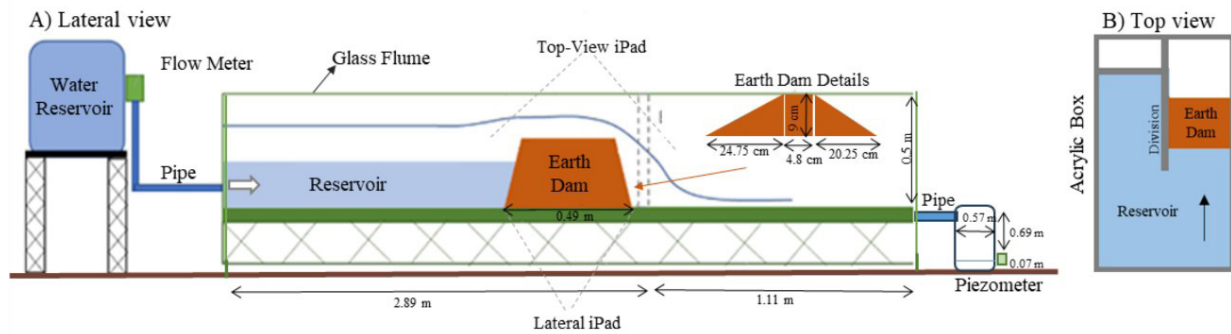


**Figure 1.** a) Lateral view of the glass flume experimental facility (not to scale); b) top view of the acrylic box.

top and at the side of the flume to capture the deformation of the dam slopes during filling, the percolation (seepage) of water downstream of the structure, and to visualize the overtopping flow process and evolution of the rupture breach. Graduated scales were glued to the right wall of the channel helping to check the filling and controlling the water depth level. The time for each process was measured using a stopwatch. The reservoir was filled by gravity in two stages to simulate a reservoir that was already operating at maximum water level (stage I), and then received an increasing inflow until the failure happened (stage II). At the end of the flume, an external reservoir (diameter 57 cm) with a capacity of 170 l collected the dam-break wave. A Sistron® piezometer was installed 7 cm from the bottom of the reservoir to record the water level every 5 s with a data logger. With these data, we determined the dam-break (rupture) hydrograph, peak flow rate ( $Q_p$ ) and peak rupture time ( $t_p$ ).

### Geometry of the earthfill dam

The height and volume of the dam (prototype) to be tested were based on the earth dam database that had accidents in 2020 and 2021 Dam Safety Reports (Agência Nacional de Águas e Saneamento Básico, 2021, 2022). The majority (77%) of these dams have a height of less than 10 m (i.e. small dams), then we adopted 9 m for the dam, with freeboard corresponding to 2 m (22% of the total height), resulting in a maximum water level of 7 m. Correlating the volumes of the reported dams with their maximum height, we obtained a power law fit with  $R^2 = 0.80$  (Von Ahn, 2023). Then, for a height 9 m, we roughly estimated the total volume of the reservoir at  $0.4419 \text{ hm}^3$ . Alzamily & Abed (2022) based their study on similar dimensions of the earth dam. Due to the structural limitations of the acrylic box used (Figure 1b), the present volume of the reservoir in the model used was  $0.27 \text{ m}^3$ . The width of the crest ( $A_c$ ) of the dam was determined using the USBR method (Centrais Elétricas Brasileiras, 2000) with a value of 4.8 m. The upstream and downstream slope ratio (mH: 1V), considered a clayey soil on the dam (Centrais Elétricas Brasileiras, 2000), resulting in a slope of 2.75 upstream ( $m_1$ ) and 2.25 downstream ( $m_2$ ).

The geometry of the model was defined based on dynamic similarity theory (Motta, 1972) and the Froude Number scales demonstrated in Julien (2002). We adopted a scale of 1:100 (Campos,

**Table 1.** Prototype based geometrical parameters for building the dam model.

Parameters	Prototype	Model
	Scale (1:100)	
Dam height ( $D_h$ )	9 m	0.9 m
Dam width ( $B_t$ )	50 m	0.5 m
Upstream slope ( $m_1$ )	2.75	
Downstream slope ( $m_2$ )	2.25	
Crest width ( $D_c$ )	4.8 m	0.048 m
Free-board ( $F_b$ )	2 m	0.02 m
Total volume ( $Vol$ )	$0.442 \text{ hm}^3$	$0.27 \text{ m}^3$

2020; Trautwein et al., 2022), mainly conditioned by the top width of the dam (0.5 m), which models a real 50 m wide dam (Table 1). In fact, dams with top width of 50 m are usual for small earth dams (Neiva Rodrigues et al., 2007).

### Soil used

The soil used to embank the earth dam was freely provided for this work including a Proctor normal test from two *in situ* samples. The Proctor normal test results in the maximum density of  $1869$  and  $1905 \text{ kg.m}^{-3}$  and the optimum soil moisture (%SM) between 11.7% and 12.4% for the two samples. These data allow us to check the degree of compaction (%C) to guarantee the maximum efficiency for the laboratory embankment (Massad, 2010; Mariano & Silva, 2022). In Brazil, the degree of compaction equal to 95%, 98% and 100% is regularly used for the construction of earth dams (Saliba, 2009).

On the other hand, Figure 2 shows the particle-size analysis of the soil using a CILAS 1180 laser particle analyzer. The material was classified as sandy silt according to the Wentworth (1922) classification with the following particle size ranges: 21.44% clay, 55.04% silt and 23.52% sand. The low content of clay present (less than 40%) creates a dam with more susceptibility to permeability and quick failure.

### Embankment Dam Construction

The construction of the dam embankment begins by delineating the dam location on the experimental flume to ensure

that the position of the dam was the same in all experiments. Also, we identified possible deformations arising from the reservoir water filling (Figure 3a).

Then, the soil was compacted inside the acrylic box, in 2-cm layers, using a free mass weight of approximately 3.5 kg (Figure 3b). Compaction was applied homogeneously from a height of 0.05 m in three cycles for each layer (Figure 3c), totaling 30 strokes (Figure 3c). At the end, the compacted dam was highlighted at the crest with a very thin layer of white limestone powder (Figure 3d), for visualization.

### Experimental plan and procedure

Three experiments were carried out differing by the inflow rate  $Q_i$  (inflow hydrograph) and, consequently, by the reservoir filling time in the two proposed stages of filling (Table 2). The first experiment (Run A) was carried out also to validate the proposed methodology. An inflow rate ( $Q_i \sim 10 \text{ L}\cdot\text{min}^{-1}$ ) was used at stage

I (filling up to 7-cm height), and after that, the inflow rate was increased to  $14 \text{ L}\cdot\text{min}^{-1}$ , representing a rapid filling from the maximum level to the failure (stage II); Run B present a higher inflow rate ( $Q_i \sim 15$  to  $20 \text{ L}\cdot\text{min}^{-1}$ ) in stage I, and reducing to  $5 \text{ L}\cdot\text{min}^{-1}$  in stage II. This reduction corresponded to less than half of the overtopped flow rate used in Run A. Run C kept the same flow rate as Run B. The only difference was that the first stage of filling was carried out until 8-cm water level. Consequently, the filling time of stage II was faster ( $\sim 340 \text{ s}$ ).

The experiments began with the reservoir filling until the maximum water level in Stage I and later, Stage II (Table 3). Two cameras recorded these processes. The time was controlled as soon as the inflowing water reached the crest of the dam and the overtopping started. As soon as the failure occurred, the reservoir valve was closed, stopping continued filling with reservoir water. Also, when failure occurred, i.e., the breach started to develop, the time of failure was registered. A mixture of water and sediment removed from the breach was transported directly

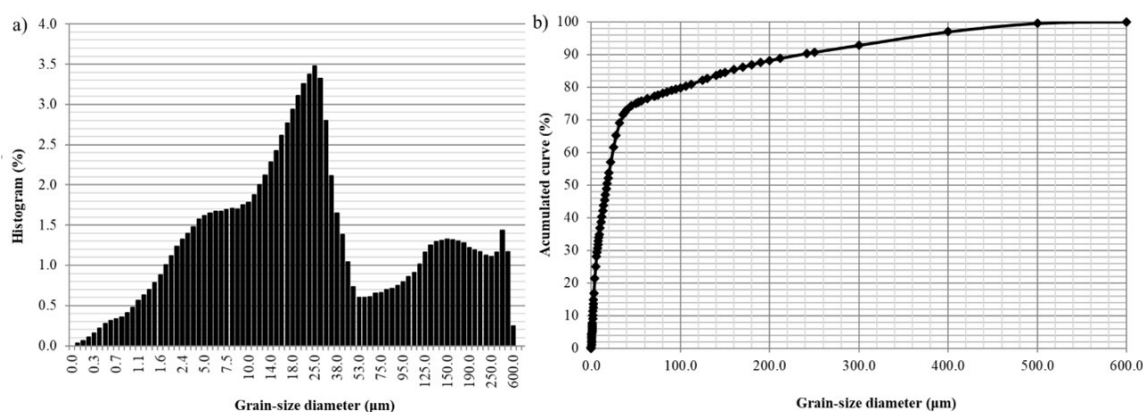


Figure 2. Grain size of the soil used in the earth dam experiments. a) histogram and b) cumulative curve.

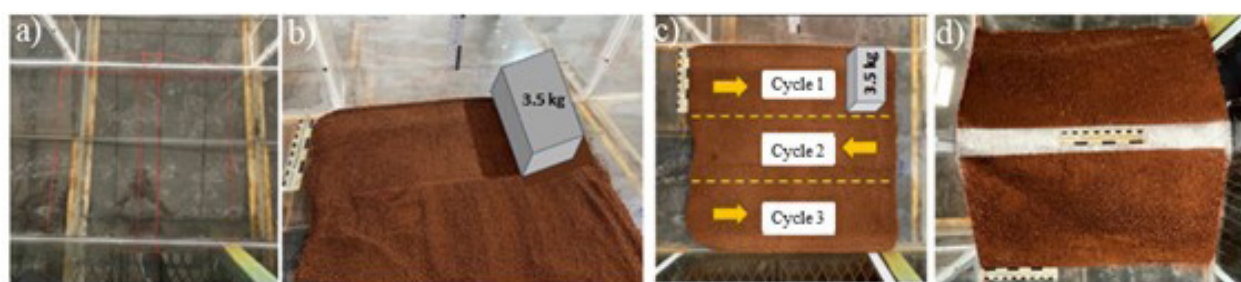


Figure 3 Embankment dam construction stages: a) delineation and location of the dam; b) compaction process; c) cycles of compaction d) the built dam.

Table 2. Inflow rate ( $Q_i$ ) and reservoir filling time for both stages of simulation.

Run	Stage I			Stage II		
	Water level (cm)	Inflow Rate ( $Q_i$ ) ( $\text{L}\cdot\text{min}^{-1}$ )	Filling time (s)	Water level (cm)	Inflow Rate ( $Q_i$ ) ( $\text{L}\cdot\text{min}^{-1}$ )	Filling time (s)
A	0-7	10.6	1220	7-9	14.33	200
B	0-7	16.3	718	7-9	5.2	760
C	0-8	17.0	857	8-9	5.0	344

**Table 3.** All experimental parameters and the upscaling for the prototype.

	Parameters	Run A		Run B		Run C	
		Model	Prot	Model	Prot	Model	Prot
Soil	Moisture (% SM)	11	-	5.9	-	14.5	-
	Density (kg.m <sup>-3</sup> )	1119	-	1324	-	1243	-
	Mean degree of compaction (% C)	63.5	-	70.0	-	69.0	-
Filling Stage I (0 to 7 or 8 cm)	Mean inflow rate Qi (L.min <sup>-1</sup> ) (m <sup>3</sup> .s <sup>-1</sup> )	10.64 (0.000177)	29.55 (17.73)	16.3 (0002717)	45.28 (27.17)	17 (0.000283)	47.21 (28.33)
	Filling time (s)	1220	12000	718	7200	1037	8400
	Water volume injected (m <sup>3</sup> )	0.215	215	0.196	196	0.241	241
	Seepage	Complete		Half		Complete	
	Mean inflow rate Qi (L.min <sup>-1</sup> ) (m <sup>3</sup> .s <sup>-1</sup> )	12.76 (0.000212)	35.43 (21.26)	5.0 (0.00008)	13.88 (8.33)	4.5 (0.000075)	12.5 (7.5)
Filling Stage II (7 or 8 to 9 cm)	Filling time (s)	200	1800	760	7800	344	3453
	Water volume injected (m <sup>3</sup> )	0.0434	43.4	0.062	62	0.0245	24.5
	Seepage	complete		completa		complete	
Failure	Overtop flow (L.min <sup>-1</sup> ) (m <sup>3</sup> .s <sup>-1</sup> )	14.33 (0.000238)	39.71 (23.83)	5.2 (0.000086)	14.45 (8.67)	5 (0.000083)	13.88 (8.33)
	Time of rupture (s)	20	200	22	220	30	300
	Empty reservoir (s)	not measured		not measured		480	4800
	Total volume injected (m <sup>3</sup> )	0.2584	258.4	0.258	258.0	0.2655	265.5
	Complete seepage time (min)	00:18:56	03:03:0	00:17:25	02:51:36	00:13:40	02:13:4
	Peak outflow Qp (L.min <sup>-1</sup> ) (m <sup>3</sup> .s <sup>-1</sup> )	170 (0.00283)	472.21 283.33	153.11 (0.00255)	425.3 (255.18)	183.7 (0.003062)	510.1 (306.1)
Dam-break Hydrograph	Time to reach peak flow (s)	23	230	30	300	20	200
	Peak duration (s)	-		20	200	20	200
	Total Soil (kg)	15.91	-	15.2	-	15.8	-
Mass balance	Retained soil (kg)	10.11	-	8.75	-	8.28	-
	Eroded soil (kg)	5.8	-	4.64	-	6.31	-
	Total soil collected (kg)	15.91	-	13.39	-	14.59	-
Breach features	Soil difference	-	-	1.81	-	1.18	-
	Position	Left wall	-	Left wall	-	Right Center	-
	Width (m)	0.23	23	0.15	15	0.27	27
	Formation time (s)	23	230	25	250	35	350

to the downstream reservoir with the measurement of the water level along time (dam-break rupture hydrograph) until the dam-break wave stopped completely, i.e. emptied the reservoir. After one day, a mass balance was carried out by dividing the sediments into two parts: the sediment retained in the dam and the sediment carried by the dam-breaking wave. Then, the materials were dried and weighted.

For all simulations, the selected soil was sieved (in 4 mm sieves - Run A, and 2 mm – Runs B and C) to break the large dry agglomerates formed. Also, the moisture of the soil was corrected close to optimum. The specific mass and degree of soil compaction were also determined. Run C presented the wettest soil and Run B the driest soil for construction of the dam (Table 3), while Run A best approached the range of values considered for optimal moisture (11.7% and 12.4%).

## RESULTS

### Reservoir filling

Figure 4a shows the inflow hydrograph and the reservoir water filling times of stages I (0-7 cm and 0-8 cm) and II (7-9 cm and 8-9 cm). After an initial flow adjustment (~60 to 120 s), the flow reached constant values. In stage I, the lowest average filling flow was Run A ( $Q_i = 10.64 \text{ L.min}^{-1}$ ), which led to shorter filling time (Figure 4b). Run B and Run C present average filling flow around  $16.3 \text{ L.min}^{-1}$  and  $17 \text{ L.min}^{-1}$  respectively, characterizing a faster reservoir water filling. Regarding the maximum flow rates, we observed that in Run B the maximum flow was  $20.0 \text{ L.min}^{-1}$  and lasted 220 s, while Run C presented a maximum flow of  $19.5 \text{ L.min}^{-1}$  with a duration of 480 s (8 min). In stage II, we observed that

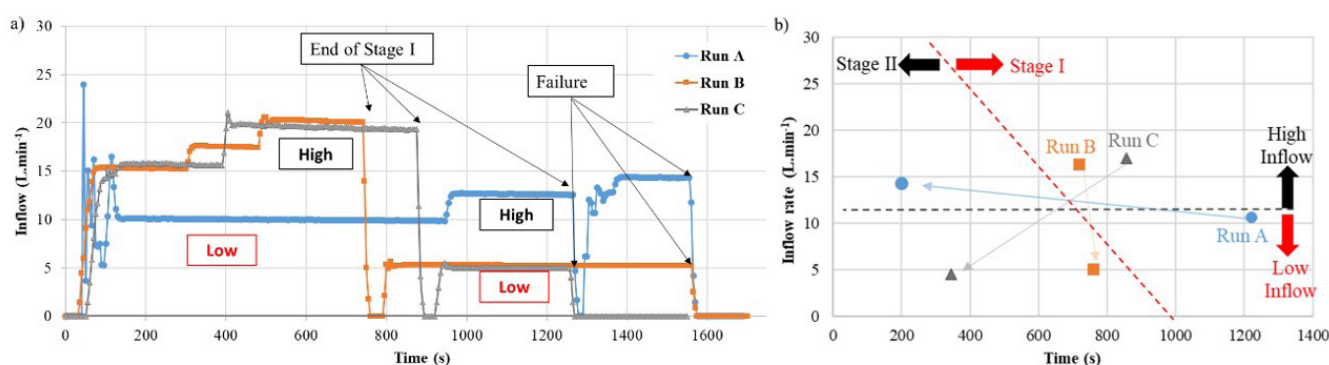


**Figure 4.** a) Time series of injected water (inflow rate); b) average values highlighting the stages of experiments and the thresholds (low and high) considered for these experiments.

the filling flow was higher for Run A ( $12.76 \text{ L}\cdot\text{min}^{-1}$ ) and lower for Run B ( $5 \text{ L}\cdot\text{min}^{-1}$ ) and Run C ( $4.5 \text{ L}\cdot\text{min}^{-1}$ ). Between Run B and Run C, there was a significant difference in filling time, with Run B taking practically twice as long to fill to the crest (760 s) compared to 344 s (05:44 min) of Run C, which had a lower inflow rate. Figure 4b summarizes these average values indicating the criteria used to classify between low and high inflows rate in the experiments.

## Seepage and deformations

Figure 5 shows the end of Stage I (Figures 5a-c) and Stage II (Figures 5d-f) of the reservoir filling. We noticed a small inclination of the water line in Run A and Run B because the glass flume was slightly inclined transversely (Figure 5a and Figure 5b). For trial C, the slope was corrected.

For Runs A and C, the dam was saturated and water percolated (indicated by the white arrow - Figure 5a and Figure 5c) below the structure before the reservoir water reached the crest of the dam. No significant deformation was observed on the dam slopes during filling of the reservoir in stage I (up to 7 cm). A small deformation was observed at the crest of the dam for Run C, with a small displacement of the central axis (sinuosity of the yellow line - Figure 5c). At stage II of filling, a small advance of the downstream slope can be seen, as indicated by the blue line in Figure 5d and Figure 5f. No water flow was observed downstream of the dam for Run B (Figure 5b). However, Figure 5e identifies the greatest deformation of the structure, where failure was due to liquefaction before overtopping (Zhang et al., 2009). However, a weak-point over the downstream slope was not observed to reach the worst-case scenario of failure of the dam. In fact, after the flow overtopped the crest and the failure breach developed, these deformations caused by liquefaction were still present in the downstream slope (see also Figure 6). We infer that deformation acted on the failure but only affected the superficial part of the downstream slope and not the internal embankment of the dam.

Water percolation (seepage) through the dam over time was captured by the lateral camera. Then, the flow lines were plotted every 1 minute (Figures 5g to 5i). The water percolated through the entire mass in 1136 s, just before the end of stage I of filling

(1220 s) in Run A. For Run B, the percolation of water in the mass was not complete (half of the dam) and corresponded to half the filling time of stage I (380 s). One of the factors that contributed to this result was the higher inflow rate applied at this stage. The complete percolation of the dam was observed only at stage II of filling ( $\sim 1045 \text{ s}$  - 17:25 min) with 8-cm water depth. Run C shows a rapid, complete percolation of water (820 s) just before the end of stage I, likely related to the higher soil moisture compared to other runs.

## Overtopping failure

Figure 6 shows the final images of stage II of reservoir water filling until the moment of overtopping occurs and then, the dam thorough failure. The process was fast, the time taken for the water line to reach the crest for failure was around 30 s (similar in all runs). The soil composition with lower content of clay explains this quick failure. Regarding the origin of the breach, Runs A and B occurred predominantly on the right side of the channel, due to a slightly transverse inclination. In Run C, the origin of the breach began in the central-left part of the dam. In fact, the rigid side-wall Run A also created two preferential paths for the passage of water (Figure 6d, white arrow at 26 s). Apart of that, the evolution of the breach underwent significant changes until approximately 30 sec after overtopping (Figure 6 - breach evolution). After this (Figure 6 - complete breach), only small changes were identified up to the complete emptying of the reservoir. Run B presented the smallest breach width ( $B_w$ ) with 15 cm, followed by Run A (23 cm) and Run C (27 cm). The breach width was larger in Run C corroborating the results signaled in the dam-break hydrograph, in which a higher peak flow ( $Q_p$ ) was observed for this run.

Figure 7 shows the inflow rates ( $Q_i$ ) values at the moment of rupture related to the time of rupture after overtopping ( $t_r$ ) and the breach width ( $B_w$ ). As the inflow rate increases, the failure occurs faster. However, the differences between Run A (higher flow rate) and Runs B and C (low flow rate) were insignificant (less than 2 s between Run A and B). The breach width shows no correlation with the inflow rate. Both results evidence that the physical characteristics of the earth dam (soil, moisture and

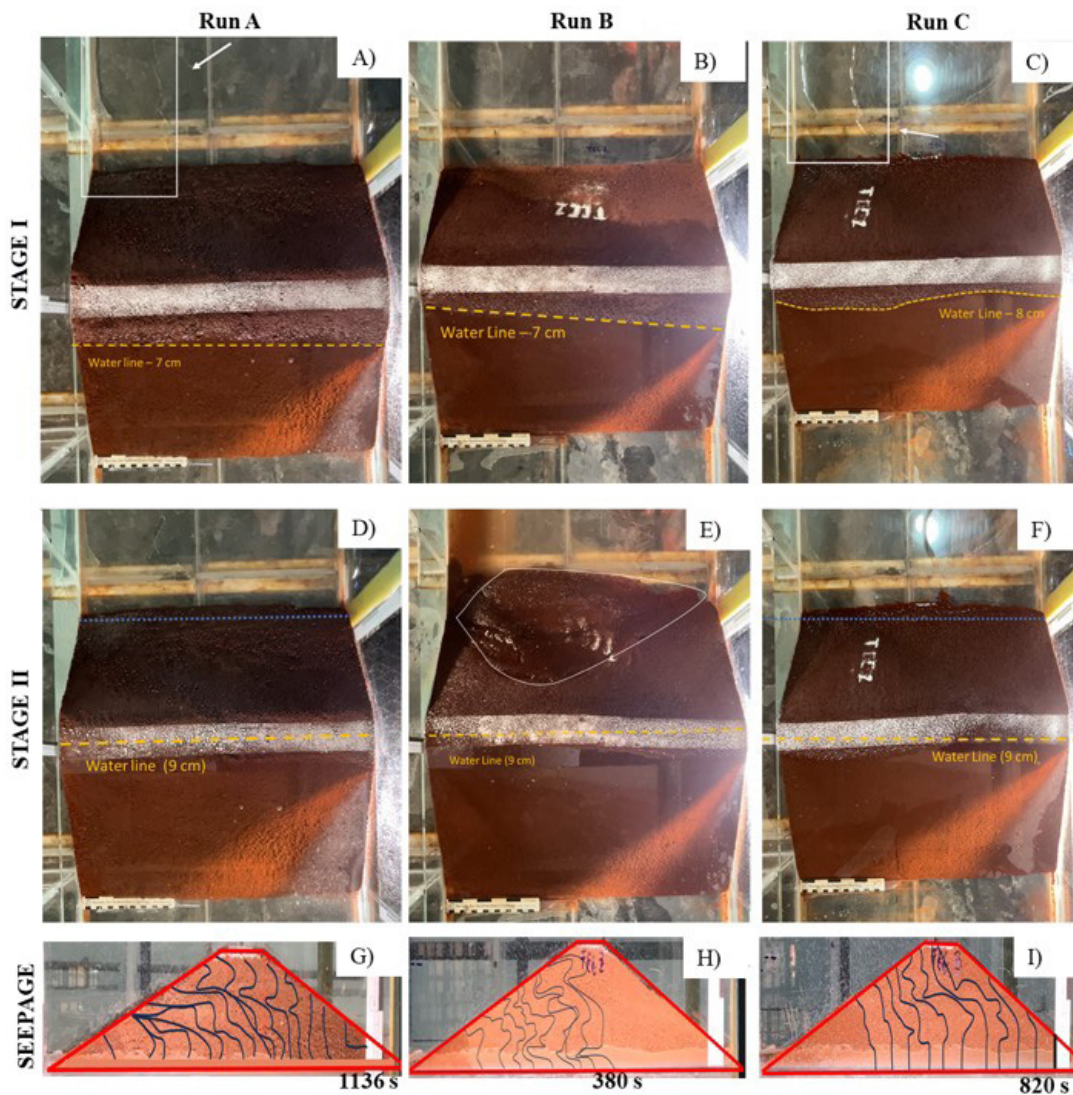


**Figure 5.** Images of the end of each stage of experiments (Stage I – a, b and c) and Stage II (d, e and f) and the seepage flow lines (g, h, and i) at every 60 s with the total time of last flow line plotted.

compaction) also contribute to the process, in addition to the inflow rate  $Q_i$ . Nonetheless, the effect of the side-walls influenced in part the opening breaching process. Pickert et al. (2011) concluded that two failure mechanisms were observed in a breaching opening: (a) constant erosion and (b) sudden collapse of the lateral slopes of the breach. The experiment here identified both mechanisms of failure on the three experiments, better evidenced on Run C that was captured by the lateral Ipad video. However the sudden collapse in Runs A and B could be minimized by the effect of the rigid side-walls (acrylic), as the breach occurs close to the left wall, comparing to central breach in Run C with developed higher values.

### Dam-break wave (rupture) hydrograph.

Figure 8 shows the dam-break (rupture) hydrograph measured for Run B and Run C for a time of 100 sec. For Run A, there is no record due to operational failure in the piezometer.

However, based on the images of the experiment, the dam and water reservoir geometry, time of failure and the size of the breach, we were able to calculate (Run A) and compare (Runs B and C) the outflow rate peak ( $Q_p$ ) for all three runs. We fit an exponential rupture hydrograph usually applied in this type of study (Barfield et al., 1981; Walther, 2000; Faria et al., 2019). Then, for Run A we estimated a  $Q_p$  around  $170 \text{ L}\cdot\text{min}^{-1}$  for a peak flow time around 23 s (Figure 8a). Run B, the peak time occurs approximately after 25 to 30 s and the peak flow was  $153.11 \text{ L}\cdot\text{min}^{-1}$ . In Run C, the peak time occurred between 20 to 23 s (10 s earlier than Run B) and the peak flow was higher ( $183.73 \text{ L}\cdot\text{min}^{-1}$ ). The duration of the peak time was the same for both Runs B and C (20 s).

Run B presented a distributed dam-break (rupture) hydrograph, in which small flow peaks were still observed at 70 and 80 s after rupture. On the other hand, Run C decreased constantly after the flow peak (Figure 8c). The lower breach width ( $B_w \sim 15 \text{ cm}$ ) of the Run B delayed the dam-break wave. After 100 s of the hydrograph, a flow rate of  $20 \text{ L}\cdot\text{min}^{-1}$  was still observed for Run B,

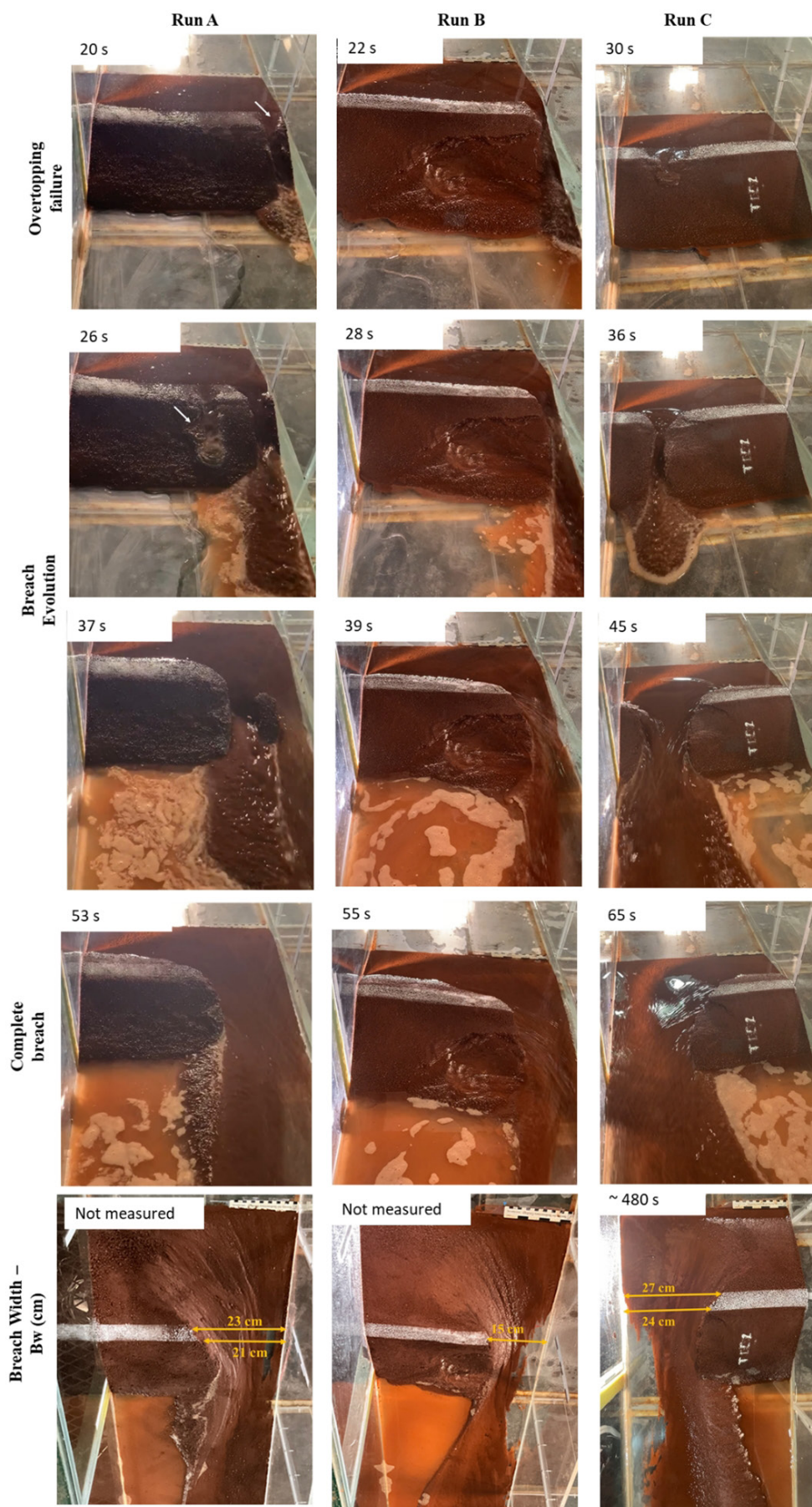
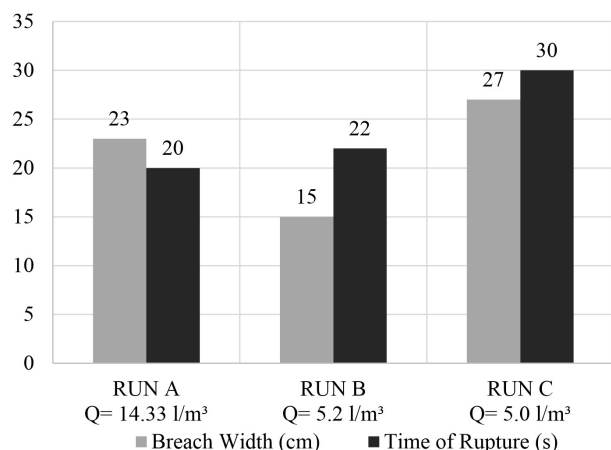
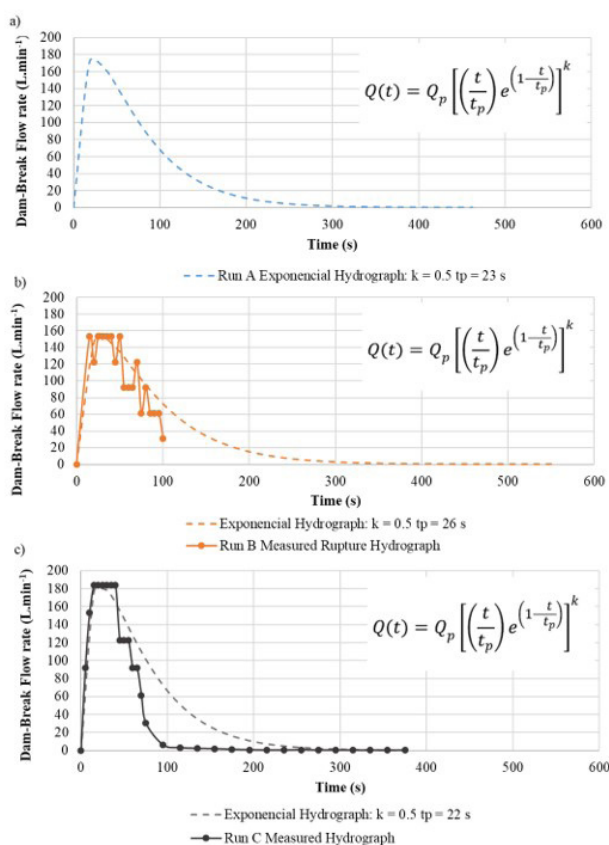


Figure 6. Overtopping dam brake failure processes and breach evolution along time.



**Figure 7.** Breach width (Bw) and time of rupture (tr) for all three experiments.



**Figure 8.** Dam-brake hydrograph for Runs B and C (solid lines) and the fit exponential-law hydrographs (dashed lines) for all runs.

while in Run C it was close to zero (Figure 8b). The total emptying time was not measured in Runs A and B, however for Run C it was close to 480 s (8 min). Yet, the measured rupture hydrograph (Runs B and C) demonstrates quicker ascent and descent phases than the exponential law usually applied in numerical modelling. These results should be further investigated.

Regarding mass balance, Run B retained more material in the dam (65%), while Run A (~63% retained) and Run C (56% retained) carried more material downstream.

The hydrograph peak flow values ( $Q_p$ ) measured were compared with current parametric equation found on literature for real dams, e.g., Lou (1981), U.S. Army Corps of Engineers (1997), United States Bureau of Reclamation (1982), Froehlich (1995), Pierce et al, (2010), as well as thick spillway equation (Chow, 1959). We observed that thick spillway equation ( $Q_p \sim 500 \text{ L}\cdot\text{min}^{-1}$ ) matches well with the upscale peak flow ( $Q_p$  between  $425 \text{ L}\cdot\text{min}^{-1}$  and  $510 \text{ L}\cdot\text{min}^{-1}$ ) obtained on the simulation (Prototype values on Table 3).

In opposite, all other equations present lower ( $Q_p \sim 100 \text{ L}\cdot\text{min}^{-1}$  on Pierce et al., 2010) or much higher values up to  $13000 \text{ L}\cdot\text{min}^{-1}$  on USBR (United States Bureau of Reclamation, 1982). Such differences are closely related to simple entry parameters (e.g. United States Bureau of Reclamation, 1982) that only consider the dam height.

### Similarity

The similarity laws were applied through derived scales of Froude number to extrapolate the observed/measured model data to a hypothetical prototype. The results are summarized in Table 3.

Most parameters reproduced in the experiments represent a real prototype as they present feasible values for real small homogeneous earthfill dams (see Rodrigues et al., 2007). The low and high dam-break wave peak flows ( $Q_p$ ) are  $255.58 \text{ m}^3\cdot\text{s}^{-1}$  (Run B  $\sim 153 \text{ L}\cdot\text{min}^{-1}$ ) and  $306.21 \text{ m}^3\cdot\text{s}^{-1}$  (Run C  $\sim 183 \text{ L}\cdot\text{min}^{-1}$ ) are compatible to natural water bodies found in Brazil (e.g. São Gonçalo channel – Rio Grande do Sul, 2022).

On the other hand, the time scale of filling and time of failure after the overtopping do not correspond to a real scale. This difference may be explained by the nature of the material used in this work, which considered low presence of clay, filters or upstream sealing. With an increase in clay content, the failure time should be longer. Nonetheless, the values obtained by methodologies usually applied FERC (Federal Energy Regulatory Commission, 1988), ELETROBRAS (Centrais Elétricas Brasileiras, 2000) equations yields 360 s (6 min), which is close to the values measures on the experiments (344 s - 5.44 min). The experimental results of Campos (2020) also present small values for the failure time than those found in the literature.

The same behaviour occurred in breach width (Bw). Applying USACE (U.S. Army Corps of Engineers, 1980), FERC (Federal Energy Regulatory Commission, 1988), ELETROBRAS (Centrais Elétricas Brasileiras, 2000) equations from several papers (Faria et al., 2019; Oliveira & Lima Neto, 2022; Machado, 2022), the values of Bw ranged from 2.7 m to 45.0 m in real dams, while the model yields 15 m to 27 m. The model values are feasible for the real earth dam.

### DISCUSSION

The physical experiments exemplified the overtopping flow accidents (failure) in smaller homogeneous earthfill dams.

The results presented here advance the understanding of how the overtopping failure process occurs in different situations. We impose the filling of the reservoir under various scenarios (low and high inflow rate) and establish qualitative results in relation to percolation (seepage) in the dam as well as their deformations during the water filling. In addition, we obtained quantitative results of measuring the inflow rate at which the structure failed, the time when the dam-break occurs, the formation and evolution of the failure breach, and finally, the dam-break (rupture) hydrograph and the amount of sediment that was carried by the dam break wave.

This work focused on the overtopping flow, but we not discard other triggers overlapping on the experiment. In fact, the sequence of seepage with subsequent saturation of the entire mass (leading to liquefaction in RUN B, for instance) could occur at the same time as overtopping flow (erosion) was acting as the main factor. Zhang et al. (2009) highlighted that 80% of all failures of earth dam are caused by overtopping or technical deficiencies (e.g. seepage and saturation). The soil used does not commonly characterize the construction of earth dams. Soil with less than 40% clay does not have the same degree of cohesion as clay and consequently presents higher permeability. Kutzner (1997) highlighted that homogeneous dams without an individual sealing element consist of cohesive soil of low permeability. In our experiments, we did not use any drainage system or upstream sealing element, representing an extreme scenario of simulation. In fact, the simulation of extreme scenarios, either physical or numerical, may be valuable to comprehend the physical process involved (Correia et al., 2018; Silva & Ribeiro, 2018; Machado, 2022). Oliveira et al. (2018) simulated seepage flow in earth dams using only sand on the dam to guarantee the kinematics scale of the process in real dams.

The initial reservoir water filling is the first test of the dam to perform the function for which it was designed (U.S. Army Corps of Engineers, 1994). Based on that, the experiments here reveal that the water percolation (seepage) in the embankment is associated with the reservoir filling time (consequently related to the inflow rate). Run B was the one that showed the shortest filling time of stage I (718 s) and no saturation of the embankment was observed for this condition. On the contrary, water percolation reached half of the massif. When percolation is excessive, instability and eventually failure of all or part of the downstream slope occurs (Stephens, 2011). In fact, this process happened on Run B-stage II, which took the longest time of filling (~760 s) and then failure occurred due to liquefaction.

The experiment simulates two different inflow rates (5 and 14 L.min<sup>-1</sup>) to establish the difference between these two scenarios. In fact, the inflow rate did not impact the time of failure significantly. These results when represented on a real scale are in the range of 3 to 5 min, faster than real dams. Besides the type of soil used in the embankment, the runs were carried out on a fixed bed model, as erosion was concentrated only at the foot of the dam (no erodible bottom). Stephens (2011) stated that this is normally associated with poor quality soils and poor compaction of the embankment. Or else, in the seal/core, trench and remedial measures can be put in place that will reduce infiltration to safe and acceptable levels. Also, the experiments also evidenced no linearity between the inflow rate (Qi) and the dam-break peak flow (Qp),

indicating the complexity related to this hydraulic phenomenon. For all three runs, failure time after the water overtopped the crest was similar.

However, it is noteworthy that Run B presented the highest degree of compaction and this was obtained with a drier soil (soil moisture of approximately 6%). In this sense, we expected that the soil moisture close to the optimum value (~12%) would present a better result in terms of dam break process (Run C). On the other hand, compaction is not only related to moisture, but also to compaction energy, which is a factor that contributed to this unexpected result. Saliba (2009) stated that the dam-breaking process is strongly dependent on the degree of compaction. The degree of compaction in Run B (higher than Runs A and C) had an impact on water percolation in the dam, which did not saturate when water filling in stage I (up to 7 or 8 cm). Also, the variation in the degree of compaction has a significant influence on the erosion rate of the dam (represented here by the breach width – Bw), showing a smaller Bw for a high degree of compaction (Run B). Consequently, a dam-break hydrograph showed low peak and less material was carried by the breaking wave. These results corroborate with Jorge (2013), who concluded that the dam-break (rupture) hydrograph is inverse to the degree of compaction. Additionally, the author observed in his experiments that the dam-break peak flow (Qp) with a lower degree of compaction (82%) was approximately double the peak flow for the degree of compaction of (95%) and the degrees of compaction of the embankments are directly related to the failure time (figure 7). Still, our degree of compaction range was smaller (Test B = 69-71% and Run C = 65-67%) than in Jorge (2013) which was 82% and 95% and similar to real dams (Saliba, 2009). The filling time, compaction and moisture soil conditions are important points to observe in physical experiments of this nature.

To better visualize graphically the effects of all these parameters together, we combine a simple relationship of the peak of dam-break flow (Qp) as a function of dam-soil parameter composed by three factors – breach width (Bw) divided by total breach (Bt) times degree of compaction (%C) and soil moisture (%SM). Figure 9 shows a linear relationship (R<sup>2</sup> = 0.99) confirming that smaller breach width (Bw) for greater degree of compaction

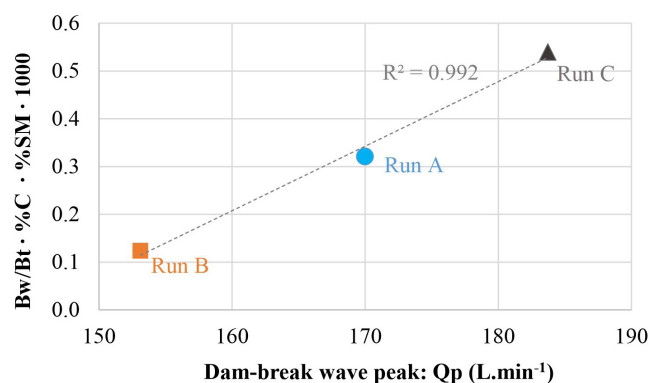


**Figure 9.** Relationship of the peak of dam-break flow (Qp) as a function of dam-soil parameter composed by three factors, i.e. breach width times degree of compaction and soil moisture.

and lower moisture led to a lower peak flow of the dam-break hydrograph (Qp). Notwithstanding, this particular correlation are based on our experiments with very few data available. We encourage further studies with more data to investigate this relationship.

Viseu et al. (2014) regard the use of physical models to modeling rupture inflow rate in dams as infrequent, because physical models should be larger. After choosing small scale values (e.g. 1:100) to avoid this disadvantage, scale effects can become more acceptable. Correia et al. (2018) complement that physical models are difficult to calibrate and the expected results are not always obtained. Despite of this, results presented here indicate that physical modeling can be used as an alternative tool for studying this phenomenon. The visualization of the process and the parameters measured (e.g. every failure time, geometries and dam-break wave hydrograph) have more advantages than disadvantages. Finally, we suggest that physical models can be used with satisfactory results as teaching tools for this type of study in agreement with Marques & Unas (2010) and Oliveira et al. (2018).

## CONCLUSION

This work sought to develop an experimental methodology that represents the real phenomenon (prototype) through a reduced model using physical modeling. The aim was to represent accidents in small homogenous earth dams. The majority of accidents occur during intense rains, with lack of information regarding these events (and Dam as well), which makes it important to understand how these parameters impact in the reservoir and earth dams. We conclude that the different temporal distributions of reservoir filling caused by low and high inflow flows simulate the failure of earth dams, mainly in relation to the saturation of the embankment. The way in which the reservoir is filled impacts how the dam will behave and this directly contributes to the formation of the breach, however, this isolated parameter is not solely responsible for the failure, which should also consider soil composition, moisture and degree of compaction.

The rupture hydrograph presents a faster descent stage than an exponential hydrograph. Simulations and models based on this law may minimize the effect of the dam-break wave, also impacting water resource decision-making for damage reduction.

Some difficulties were encountered in carrying out the proposed physical simulations, however the simulated extreme scenarios, i.e., less cohesive material with no filter/drain and sealant layer, cause a rapid saturation of the dam. In consequence, the triggering mechanism of the dam failure combine overtopping flow and liquefaction as well. The attempt to isolate each phenomena (overtopping or liquefaction) is a challenge. Using a clayey soil, or even adding filters and sealant layer can improve the results as well as present methodology.

The differences between the model results and the real ones (prototype) are inherent to the physical modeling. Nonetheless, the dam-break failure caused by overtopping phenomenon has great potential to be studied via this study tool provides support for understanding the phenomenon and enrich the present state of the art.

## ACKNOWLEDGEMENTS

The authors acknowledge Dobil Engenharia Ltda for the soil supply and lab tests for the experiments. Also, authors are thankful to the Neced team and UFRGS for allowing the use of the laboratory facilities and support throughout the undergraduate studies of the first author. Finally, the authors wish to express their gratitude to Léo A. Hartmann for his assistance and comments during the preparation of this manuscript.

## REFERENCES

- Agência Nacional de Águas e Saneamento Básico – ANA. (2021). *Relatório de segurança de barragens 2020*. Brasília: ANA. Retrieved in 2023, January 30, from <https://www.snisb.gov.br/portal-snisb/documentos-e-capacitacoes/rsb>
- Agência Nacional de Águas e Saneamento Básico – ANA. (2022). *Relatório de segurança de barragens 2021*. Brasília: ANA. Retrieved in 2023, January 19, from <https://www.snisb.gov.br/portal-snisb/documentos-e-capacitacoes/rsb>
- Alzamily, Z. N., & Abed, B. S. (2022). Experimental and theoretical investigations of seepage reduction through zoned earth dam material with special core. *Materials Today: Proceedings*, 61(Pt 3), 998-1005. <http://dx.doi.org/10.1016/j.matpr.2021.10.283>.
- Aureli, F., Maranzoni, A., & Petaccia, G. (2021). Review of historical dam-break events and laboratory tests on real topography for the validation of numerical models. *Water (Basel)*, 13(14), 1968. <http://dx.doi.org/10.3390/w13141968>.
- Aureli, F., Maranzoni, A., Petaccia, G., & Soares-Frazão, S. (2023). Review of experimental investigations of dam-break flows over fixed bottom. *Water (Basel)*, 15(6), 1229. <http://dx.doi.org/10.3390/w15061229>.
- Barfield, B. J., Warner, R. C., & Haan, C. T. (1981). *Applied hydrology and sedimentology for disturbed areas* (pp. 104-108). Oklahoma: Oklahoma Technical Press.
- Bassel, B. (1904). *Earth dams: a study* (98 p.). New York: The Engineering News Publishing Company.
- Campos, R. G. D. (2020). *Proposta de uma metodologia para obtenção de parâmetros de brechas em rupturas de barragens em cascata utilizando modelagem física* (Tese de doutorado). Escola de Engenharia, Universidade Federal de Minas Gerais, Belo Horizonte. Retrieved in 2023, September 15, from <https://repositorio.ufmg.br/handle/1843/46264>
- Centrais Elétricas Brasileiras - Eletrobras. (2000). *Diretrizes para estudos e projetos de Pequenas Centrais Hidrelétricas* (Vol. 21, 199 p.). Rio de Janeiro: Eletrobras. Retrieved in 2023, September 23, from [www.eletrobras.com.br](http://www.eletrobras.com.br)
- Chow, V. T. (Ed). (1959). *Open-channel hydraulics*. Illinois: McGraw Hill Book Company.

- Collischonn, W., & Tucci, C. E. M. (1997). Análise do rompimento hipotético da barragem de Ernestina. *RBRH*, 2(2), 191-206. <http://dx.doi.org/10.21168/rbrh.v2n2.p191-206>.
- Correia, K. R., Miranda, T. C., Oliveira, C. M. M., & Teixeira, M. B. (2018). Análise de permeabilidade em modelo reduzido de barragem através da altura piezométrica. *Engineering and Science*, 6(2), 32-42. <http://dx.doi.org/10.6008/CBPC2318-3055.2018.002.0004>.
- Duarte, J. M., Blanco, C. J. C., & Santana, L. R. (2021). Estimativa de vazão máxima para projetos de barragem na bacia hidrográfica do rio uraim em paragominas/Pa. *Revista Gestão & Sustentabilidade Ambiental*, 10(1), 262-281. <https://doi.org/10.19177/rgsa.v10e12021262-281>.
- Faria, F. L. F., Silva, M. B. S., Reis, M. M., & Amorim, J. C. C. (2019). Metodologia para obtenção do hidrograma para simulação de ruptura de barragens. *Revista Militar de Ciência e Tecnologia*, 36(3), 31-37.
- Federal Energy Regulatory Commission - FERC. (1988). *Notice of revised emergency action plan guidelines* (31 p.). USA: FERC.
- Fonseca, M. E. (2021). *Análise de deformação vertical de uma barragem de terra para diferentes fases do enchimento do reservatório: estudo de caso da Barragem Pias* (Trabalho de Conclusão de Curso). Centro Tecnológico, Universidade Federal de Santa Catarina, Florianópolis.
- Franca, M. J. R. P. (2002). *Caracterização e Modelação numérica e experimental da ruptura provocada por galgamento de barragens de enrocamento* (Tese de mestrado). Instituto Superior Técnico, Universidade Técnica de Lisboa, Lisboa.
- Froehlich, D. C. (1995). Peak outflow from breached embankment dam. *Journal of Water Resources Planning and Management*, 121(1), 90-97. [http://dx.doi.org/10.1061/\(ASCE\)0733-9496\(1995\)121:1\(90\)](http://dx.doi.org/10.1061/(ASCE)0733-9496(1995)121:1(90)).
- Gaioto, N. (2003). *Introdução ao projeto de barragens de terra e de enrocamento*. São Carlos: EESC-USP.
- Galeano, J. C. (2016). *Estimativa de hidrogramas e propagação de onda de cheia proveniente da ruptura hipotética de pequenas barragens* (Trabalho de diplomação). Departamento de Engenharia Civil, Escola de Engenharia, Universidade Federal do Rio Grande do Sul, Porto Alegre.
- Guireli Netto, L., Gandolfo, O. C. B., Malagutti Filho, W., Moreira, J. C. A., & Camarero P. L. (2020). A utilização de métodos geofísicos na investigação de uma pequena barragem de terra. *Boletim SBGf*, 112, 12-15.
- Hanson, G. J., Cook, K. R., & Hunt, S. L. (2005). Physical modeling of overtopping erosion and breach formation of cohesive embankments. *Transactions of the ASAE. American Society of Agricultural Engineers*, 48(5), 1783-1794.
- Jansen, R. B. (Ed.) (1983). *Dams and public safety*. USA: U.S. Department of the Interior, Bureau of Reclamation.
- Jorge, R. (2013). *Rotura de barragens de aterro por galgamento. Ensaios experimentais com aterros homogêneos* (Dissertação de mestrado). Faculdade de ciências, Departamento de Engenharia, Geografia, Geofísica e Energia, Universidade de Lisboa, Lisboa.
- Julien, P. Y. (2002). *River mechanics* (434 p.). Cambridge: Cambridge University Press.
- Kutzner, C. (1997). *Earth and Rockfill Dams. Principles of design and construction* (342 p.). Rotterdam: A.A. Balkema.
- Lou, W. C. (1981). *Mathematical modeling of earth dam breaches* (Tese de doutorado). Universidade do Estado do Colorado, Colorado.
- Luo, Y., Chen, L., Xu, M., & Huang, J. (2014). Breaking mode of cohesive homogeneous earth-rock-fill dam by overtopping flow. *Natural Hazards*, 74, 527-540. <http://dx.doi.org/10.1007/s11069-014-1202-8>.
- Machado, W. P. R. (2022) *Utilização de metodologia simplificada para avaliação de ruptura hipotética de barragens-estudo de caso: UHE Pedra do Cavalo-(BA)* (Trabalho de conclusão de curso). Instituto de Pesquisas Hidráulicas da Universidade Federal do Rio Grande do Sul, Porto Alegre.
- Mariano, D. C. L., & Silva, J. B. (2022). Barragens de terra: características de seus alteamentos. *Research, Social Development*, 11(11), e277111133469. <http://dx.doi.org/10.33448/rsd-v11i11.33469>.
- Marques, J. C., & Unas, M. (2010). Estudos em modelo reduzido de percolação em barragens de aterro. In *Jornadas de Hidráulica, Recursos Hídricos e Ambiente* (pp. 1-7). FEUP.
- Massad, F. (Ed.) (2010). *Obras de terra: curso básico de geotecnia*. São Paulo: Oficina de Textos.
- Motta, V. F. (1972). *Curso de teoria da semelhança* (154 p.). Porto Alegre: Ed. URS.
- Neiva Rodrigues, L., Eyji Sano, E., de Azevedo, J. A., & Medrado da Silva, E. (2007). Distribuição espacial e área máxima do espelho d'água de pequenas barragens de terra na bacia do Rio Preto. *Revista Espaço e Geografia*, 10(2), 379-400. Retrieved in 2024, January 14, from <https://periodicos.unb.br/index.php/espacoegografia/article/view/39807>
- Oliveira, L. C. S., & Lima Neto, I. E. (2022). Simulação do rompimento de barragens em cascata em uma bacia hidrográfica semiárida. *Revista DAE*, 70(235), 203-216.
- Oliveira, T. C. F. O., Dezen, B. G. S., Dahmer, R. R., Antonio, I. O., & Ortega, J. C. B. O. (2018). Avaliação de modelos físicos reduzidos construídos em laboratório para o estudo da percolação de água em duas barragens homogêneas de terra. In *Anais do XIX Congresso Brasileiro de Mecânica dos Solos e Engenharia Geotécnica Geotecnia e Desenvolvimento Urbano*. Salvador.

- Pereira, G. M. (2017). *Descrição de casos de rupturas de barragens A partir da década de 50, em âmbito mundial* (Dissertação de mestrado). Universidade Federal Fluminense, Rio de Janeiro.
- Pickert, G., Weitbrecht, V., & Bieberstein, A. (2011). Breaching of overtopped river embankments controlled by apparent cohesion. *Journal of Hydraulic Research*, 49(2), 143-156.
- Pierce, M. W., Thornton, C. I., & Abt, S. R. (2010). *Predicting peak outflow from breached embankment dams. National Dam Safety Board Steering Committee on Dam Breach Equations*. Fort Collins: Colorado State University.
- Rio Grande do Sul. Secretaria do Meio Ambiente e Infraestrutura - SEMA. (2022). *Grupo de Trabalho de Segurança de Barragens. Relatório de Atividades de 2022*. Porto Alegre: SEMA.
- Rodrigues, L. N., Sano, E. E., Azevedo, J. A., & Silva, E. M. (2007). Distribuição Espacial e Área Máxima do Espelho d'água de Pequenas Barragens de Terra na Bacia do Rio Preto. *Espaço e Geografia*, 10(2), 379-400. Retrieved in 2024, January 14, from <https://www.researchgate.net/publication/228651957>
- Saliba, A. P. M. (2009). *Uma nova abordagem para análise de ruptura por galgamento de barragens homogêneas de solo compactado* (Tese de doutorado). Programa de Pós-graduação em Saneamento, Meio Ambiente e Recursos Hídricos, Universidade Federal de Minas Gerais, Belo Horizonte.
- Silva, A. F. R., & Ribeiro, C. B. M. (2018). Estudo dos hidrogramas formados por e galgamento para propagação de onda de cheia proveniente de ruptura de barragem-estudo de caso: barragem de Chapéu d'uvas-Mg. In *III Simpósio de Recursos Hídricos da Bacia do Rio Paraíba do Sul Juiz de Fora/MG*. ABRHidro.
- Stephens, T. (2011). *Manual sobre pequenas barragens de terra-Guia para a localização, projeto e construção*. Roma: Food and Agriculture Organization of the United Nations.
- Trautwein, D., Guimarães, A. G., & Tiago Filho, G. L. . (2022). Simulação e estudo das deformações que precedem o rompimento de barragens através de modelo reduzido (v. 4, p. 21-31). In O. S. Guimarães (Org.), *Engenharia, Gestão e Inovação*. Belo Horizonte: Poisson.
- U.S. Army Corps of Engineers – USACE. (1980). *Flood emergency plans, guidelines for corps dams* (57 p). Washington: Department of the Army, Hydrologic Engineering Center.
- U.S. Army Corps of Engineers – USACE. (1994). *Engineering and design earth and rock-fill dams-general design and construction considerations*. Washington: Department of the Army, U.S. Army Corps of Engineers.
- U.S. Army Corps of Engineers – USACE. (1997). *Hydrologic engineering requirements for reservoirs* (115 p). Washington: Department of the Army, Hydrologic Engineering Center.
- United States Bureau of Reclamation – USBR. (1982). Reclamation planning instruction. In United States Bureau of Reclamation – USBR. *Guidelines for Defining Inundated Areas Downstream from Bureau of Reclamation Dams* (Nº 82-11). Denver: United States Department of Interior.
- Viseu, M. T., Almeida, A. B., & Franco, A. B. (2014). Integration of computational and experimental models for dam break flood risk analysis. *International Journal of Safety and Security Engineering*, 4(1), 1-18.
- Von Ahn, B. (2023). *Experimentos físicos de barragens de terra homogênea sujeitas ao galgamento* (Trabalho de conclusão de curso). Instituto de Pesquisas Hidráulicas, Universidade Federal do Rio Grande do Sul, Porto Alegre. Retrieved in 2024, January 14, from <http://hdl.handle.net/10183/264949>
- Walther, P. E. M. (2000). Appropriate technology: simplified dam failure analysis using spreadsheet computations. In *Western Regional Conference* (9 p.). Portland.
- Wentworth, C. K. (1922). A scale of grade and class terms for clastic sediments. *The Journal of Geology*, 30(5), 377-392. <https://doi.org/10.1086/622910>.
- World Commission on Dams. (2000). *Dams and development: a new framework for decision-making: the report of the world commission on dams*. United Kingdom: Earthscan.
- Wylam, K. E. (2016). *Hazard potential classification assessment for the CCR impoundment*. Iowa: MidAmerican Energy Company, Louisa Generating Station.
- Zhang, L. M., Xu, Y., & Jia, J. S. (2009). Analysis of earth dam failures: a database approach. *Georisk*, 3(3), 184-189. <http://dx.doi.org/10.1080/17499510902831759>.

### Authors contributions

Bianca dos Santos Von Ahn: Developed the experiments, writing the text and prepare figures.

Rafael Manica: Supervised the experimental work, writing and translated the manuscript.

**Editor-in-Chief:** Adilson Pinheiro

**Associated Editor:** Iran Eduardo Lima Neto